CSIRO PUBLISHING

International Journal of Wildland Fire **2019**, *28*, 308–326
https://doi.org/10.1071/WF18089

The FireFlux II experiment: a model-guided field experiment to improve understanding of fire–atmosphere interactions and fire spread

Craig B. Clements[A,L], *Adam K. Kochanski*[B], *Daisuke Seto*[A], *Braniff Davis*[A], *Christopher Camacho*[A], *Neil P. Lareau*[A], *Jonathan Contezac*[A], *Joseph Restaino*[C], *Warren E. Heilman*[D], *Steven K. Krueger*[B], *Bret Butler*[E], *Roger D. Ottmar*[F], *Robert Vihnanek*[F], *James Flynn*[G], *Jean-Baptiste Filippi*[H], *Toussaint Barboni*[H], *Dianne E. Hall*[A], *Jan Mandel*[I], *Mary Ann Jenkins*[B], *Joseph O'Brien*[J], *Ben Hornsby*[J] *and Casey Teske*[K]

[A]Fire Weather Research Laboratory, Department of Meteorology and Climate Science, San José State University, San José, CA 95192, USA.
[B]Department of Atmospheric Sciences, University of Utah, Salt Lake City, UT 84112, USA.
[C]School of Environmental and Forest Sciences, University of Washington, Seattle, WA 98195, USA.
[D]USDA Forest Service Northern Research Station, Lansing, MI 48910, USA.
[E]USDA Forest Service, Fire Sciences Laboratory, Missoula, MT 59808, USA.
[F]USDA Forest Service Pacific Northwest Research Station, Seattle, WA 98103, USA.
[G]Department of Earth and Atmospheric Sciences, University of Houston, Houston, TX 77204, USA.
[H]University of Corsica, 20250 Corte, France.
[I]Department of Mathematical and Statistical Sciences, University of Colorado Denver, Denver, CO 80204, USA.
[J]USDA Forest Service, Southern Research Station, Athens, GA 30602, USA.
[K]University of Montana, Missoula, MT 59812, USA.
[L]Corresponding author. Email: craig.clements@sjsu.edu

Abstract. The FireFlux II experiment was conducted in a tall grass prairie located in south-east Texas on 30 January 2013 under a regional burn ban and high fire danger conditions. The goal of the experiment was to better understand micrometeorological aspects of fire spread. The experimental design was guided by the use of a coupled fire–atmosphere model that predicted the fire spread in advance. Preliminary results show that after ignition, a surface pressure perturbation formed and strengthened as the fire front and plume developed, causing an increase in wind velocity at the fire front. The fire-induced winds advected hot combustion gases forward and downwind of the fire front that resulted in acceleration of air through the flame front. Overall, the experiment collected a large set of micrometeorological, air chemistry and fire behaviour data that may provide a comprehensive dataset for evaluating and testing coupled fire–atmosphere model systems.

Received 26 January 2018, accepted 4 January 2019, published online 23 April 2019

Introduction

The relationship between fire spread, wind and fuel properties has been an area of research for many decades (Rothermel 1972; Cheney *et al.* 1993; Sullivan 2009). Increased understanding of the fundamental physical processes associated with fire and its interactions with the atmosphere allowed the development of a wide class of fire and smoke models, many of which became useful tools routinely utilised by fire managers, such as FARSITE (Finney 1998), BEVAVE (Andrews 2014) and DaySmoke (Achtemeier *et al.* 2011). As fire behaviour and smoke models evolve, so do requirements in terms of data for their validation. Models have become more complex, aiming at better representation of the physical process driving fire progression and plume development, which results in increasing demand for datasets for assessing whether these processes are rendered realistically.

The history of fire experiments conducted in an open environment allowing natural plume development goes back to the 1950s (e.g. Schroeder and Countryman 1960; Taylor *et al.* 1973; FIRESCAN Science Team 1996; Stocks *et al.* 1996). Here, we present just a handful of experiments with the intention to illustrate the change in the scope of wildfire observations rather than to provide an exclusive list of all experimental burns conducted over the last five decades. Fire experiments during Project Flambeau were aimed at providing descriptive information on the behaviour of fire plumes based on experimental burns using piles of various fuels that were instantaneously ignited under weak wind conditions (Countryman 1969; Palmer 1981). The Euroka experiment, conducted in Queensland, Australia (Adams *et al.* 1973), complemented the initial efforts of Project Flambeau by providing measurements of the wind speed, temperature and radiant energy within and around a 20.2-ha mass fire. The 1989 Canadian Mass Fire Experiment (Stocks and McRae 1991; Quintiere 1993; McRae 1996) provided a comprehensive set of observations including 10-m winds, air temperature, gas concentrations (O_2, CO_2 and CO), fuel consumption estimates, airborne analyses of the gases and particles within the plume and infrared imagery of the fire front. Stereo photography was also used to estimate the plume height, while multiple soundings provided ambient vertical meteorological profiles. One of the biggest deficiencies of this experiment was associated with limited observations of the fire dynamics. The sparseness of surface observations, the randomness in fuel distribution and the complicated spiral ignition that was used resulted in a complex flame pattern that was very hard to analyse (Quintiere 1993). Despite these limitations, this experiment laid the foundation for future integrated fire experiments.

Understanding the needs of the surface fire models available at that time, Cheney *et al.* (1993) and Cheney and Gould (1995) collected multiple observations of the rate of spread of grass fires under various wind and fuel conditions. These experiments were designed for uncoupled one-dimensional fire-spread models driven by the near-surface wind speed, so meteorological data collected during these experiments were generally limited to 2-m wind speeds measured at the corners of the burn unit. Even though the focus of these experiments was the general characteristics of the fire progression, and no data were collected that would allow examining fire–atmosphere interactions or the plume dynamics, this dataset served as a reference point for the wildland–urban interface (WUI) Fire Dynamics Simulator (WFDS), a coupled fire–atmosphere modelling system (Mell *et al.* 2007).

In order to provide scientific insight into intense wildland fires and to support the development of crown fire models, the International Crown Fire Modelling Experiment (ICFME) was conducted near Fort Providence, North-west Territories, Canada, from 1997 to 2001 (Stocks *et al.* 2004). The experiment provided extensive measurements of thermal radiation, vertical temperature profiles in and above the advancing flame front, fire spread patterns, spotting distances and densities, flame front residence times, flame size and geometry, and fuel moisture. Unfortunately, the small size of the experimental plots (only 2.25 ha on average) and the lack of comprehensive micrometeorological observations near the fire and in the plume column limited its value as a benchmark dataset for validating coupled fire–atmosphere models. Natural fire runs during ICFME lasted only a couple of minutes, which was too short to allow a thorough investigation of the effects of the fire–atmosphere coupling on fire propagation and plume development, which are crucial from the coupled fire-modelling standpoint. Nevertheless, the data collected during this experiment benefited the future development of coupled models. For instance, the original estimate of the heat extinction depth used in WRF-SFIRE (Mandel *et al.* 2011) comes from this experiment and these data allowed the first crown fire evaluation of FIRETEC (Linn *et al.* 2012).

The ICFME was followed by the FROSTFIRE experiment conducted in the boreal forest region of Alaska, which focused on 'the impacts of weather and vegetation on fire behaviour and the resulting effects of fire on feedbacks to climate' (Hinzman *et al.* 2003). This extensive experiment, covering a 970-ha subbasin of the Caribou–Poker Creeks Research Watershed, provided insight into the fire–soil interactions and vegetation recovery in a permafrost-dominated landscape. Unfortunately, the lack of micrometeorological observations near the fire and in the plume, as well as the ignition procedure involving multiple sequentially ignited strips, limited its usefulness from the coupled fire–atmosphere modelling standpoint.

A series of experiments were conducted to investigate dry eucalypt fires during Project Vesta in Australia. During the summers of 1998, 1999 and 2001, a total of 104 experimental fires (200 × 200-m units covering a range of fuel ages and characteristics) were lit under moderate and high fire-danger conditions (Gould *et al.* 2007; Cheney *et al.* 2012). One of the unique aspects of the latter project was its focus on replicability between experiments. During the burn days, multiple burn units were ignited at the same time in order to provide replication and minimise the impact of variable weather conditions on fire behaviour.

In coupled fire–atmosphere models, the fire rate of spread at any point in the model domain is computed from local winds as opposed to uncoupled models that utilise ambient winds. Therefore, the local fire-affected meteorology (including both fire-induced horizontal winds and fire-induced updrafts) becomes a key element needed for model validation. With coupled fire–atmosphere models in mind, the initial FireFlux experiment was conducted (Clements *et al.* 2007). This experimental burn of ~32 ha of flat grass prairie provided the first observations of the turbulent fluxes of heat, moisture and momentum in the fire environment. Two towers, equipped with sonic anemometers and thermocouples, were placed in the burn unit. The fire, ignited along the upwind edge of the burn unit, was allowed to propagate freely through the prairie and passed the meteorological towers where vertical profiles of the three-dimensional wind velocities, temperatures and moisture were measured. Despite the limitations of this campaign, including the lack of continuous infrared (IR) fire-front progression history and plume-height observations, this experiment became the most widely used dataset for validation of coupled fire–atmosphere models such as FIRETEC (Dupuy *et al.* 2014), MesoNH (Filippi *et al.* 2013), WRF-SFIRE (Kochanski *et al.* 2013) and Rabbit Rules (Achtemeier 2013).

Another recent large-scale project aimed at providing a comprehensive model evaluation dataset for fire behaviour models was the RxCADRE (Prescribed fire Combustion,

Atmospheric Dynamics Research Experiment) project conducted in Florida longleaf pine stands in 2012 (Ottmar *et al.* 2016). The RxCADRE multidisciplinary team of scientists conducted 12 separate experimental grass and forest burns, during which fuel, meteorology, fire behaviour and ecological effects, as well as chemical smoke composition, were sampled. One of the biggest limitations of this dataset relates to the selection of burn units. Out of the total of 12 burns, 9 were conducted in very small burn units (100 × 200 m; 2 ha), which were ignited using hand-held drip torches, whereas the remaining units were 200 and 400 ha in size and ignited using drip torches mounted on all-terrain vehicles. Even though RxCADRE provided unprecedented comprehensive datasets, limited micrometeorological observations (Clements *et al.* 2016), the low intensity of the experimental burns, their small sizes and their short durations severely limit the usefulness of RxCADRE data for the validation and development of coupled fire–atmosphere models operating on numerical grids with spacings of tens to hundreds of metres.

The need for a comprehensive observational dataset characterising fire progression, plume evolution and the atmospheric circulations formed near the fire line motivated the authors of the present paper to revisit the FireFlux site (Clements *et al.* 2007), and conduct a follow-up, more comprehensive measurement campaign called FireFlux II (FF2), targeted at filling gaps in the original FireFlux dataset and providing additional insight into the nature of fire–atmosphere interactions and fire-induced turbulence regimes that develop in the vicinity of spreading fires. In the next section of this paper, we present the experimental design of the FF2 experiment and describe how high-resolution coupled modelling was utilised in the planning stage of the experiment. The following section describes some key results obtained from various measurement systems, and is followed by concluding remarks providing a summary of the successes and limitations of this study.

Experimental design

Experimental area and instrumentation overview

Although the site has been described in detail by Clements *et al.* (2007), a short description is provided here. The FF2 campaign was conducted on 30 January 2013 at the same prairie site as the 2006 FireFlux experiment. The prairie is located at the University of Houston Coastal Center (HCC) in Galveston County near La Marque, Texas, ~45 km south-east of Houston and 22 km north-west of Galveston Bay. The prairie (Fig. 1), at 40 ha (0.40 km^2) and 5 m above mean sea level (MSL), is categorised as a Texas Gulf Coast tall grass prairie, consisting mostly of native tall grasses. The area is typically managed by annual mowing and prescribed burning every 2–5 years. It was last burned during the first FireFlux experiment in 2006.

The experimental design was aimed at allowing a head fire to move freely through an elaborate instrumentation array designed to sample both the near-surface atmospheric conditions and corresponding fire behaviour. The instrument platforms included towers, *in situ* fireproof sensors, remote sensing platforms and one airborne platform. A detailed description of the meteorological instrument platforms and sensors is included in Table 1, and the experimental layout is shown in Fig. 1.

Atmospheric measurements

The key surface meteorological platforms included an array of towers. A permanent 43-m meteorological tower is situated in the middle of the northern half of the burn unit (Figs 1 and 2). Additionally, three 10-m meteorological towers were installed in the burn unit in a diamond array south of the 43-m tower (Figs 1 and 3*j*). Each tower held a suite of meteorological instruments designed to measure near-surface momentum and heat transport before, during and after the fire front passage (FFP). The 3-D sonic anemometers (Applied Technology, Inc., SATI-Sx and RM Young 81000 models) on the towers provided the east–west (u), north–south (v) and vertical (w) wind velocity components, and the sonic temperatures T_s. The sonic anemometers were sampled at a rate of 10 Hz using Campbell Scientific, Inc. (CSI) CR1000 and CR3000 data loggers. The sonic anemometers were mounted 5.8, 10, 20 and 43 m above ground level (AGL) on the 43-m tower and 5.3 m AGL on each 10-m tower. Unfortunately, the sonic anemometer data from the 43-m level was not recorded owing to a malfunction in the data logging system. To measure high-frequency thermodynamic profiles associated with the near-surface plume, thermocouple arrays were mounted on each tower with thermocouples placed at 1-m intervals. The fine-wire thermocouples (Table 1, Omega, Inc.) were sampled at a rate of 1 Hz. Barometric surface pressure was also measured 3 m AGL on each tower using RM Young 61302V barometric pressure sensors. Heat flux radiometers (Medtherm, 64 series) were mounted at a height of 4.6 m AGL on the short towers to measure the emitted radiation from the fire front. The southern short tower was equipped with an additional total heat flux sensor (Hukseflux, SBG01), which measures the convective components in addition to the radiative heat flux. The radiometers were oriented nadir, facing downward in order to measure the radiative heat flux being emitted vertically from the fire. Two additional dual-band radiometers were mounted 5.8 and 10 m AGL on the 43-m tower. Each tower was equipped with a Global Positioning System (GPS) receiver to ensure synchronised time stamping of data between towers. Each tower base and sonic anemometer electronics box was wrapped in a fire-resistant material, which allowed the instruments and the data loggers to operate in the extreme heat during FFP. Surface winds were measured around the burn unit perimeter using 24 cup-vane anemometers (Onset Corp., S-WMA-M003), spaced ~20 m apart at a height of 3.3 m (Figs 1, 3*i*). Each perimeter anemometer collected wind speed and direction data at 0.3 Hz.

The California State University Mobile Atmospheric Platform System (CSU-MAPS) (Clements and Oliphant 2014) 32-m micrometeorological tower (Fig. 3*b*) was located on the south-east corner of the burn unit and collected thermodynamic and wind profiles using 3D and 2D sonic anemometers (RM Young, 81000 and Gill Instruments, Ltd, Windsonic), and Vaisala, Inc., HMP45C temperature and relative humidity probes. Other instrumentation outside the burn unit included two Doppler sodars that provided 10-min average vertical wind profiles. One sodar (Atmospheric Research & Technology, VT-1; Fig. 3*h*) was located on the north-west corner of the burn unit ~400 m north-west of the ignition line, whereas the second was installed 20 m north-west of the ignition line and 100 m north-west of the 43-m tower, near the University of Houston Atmospheric

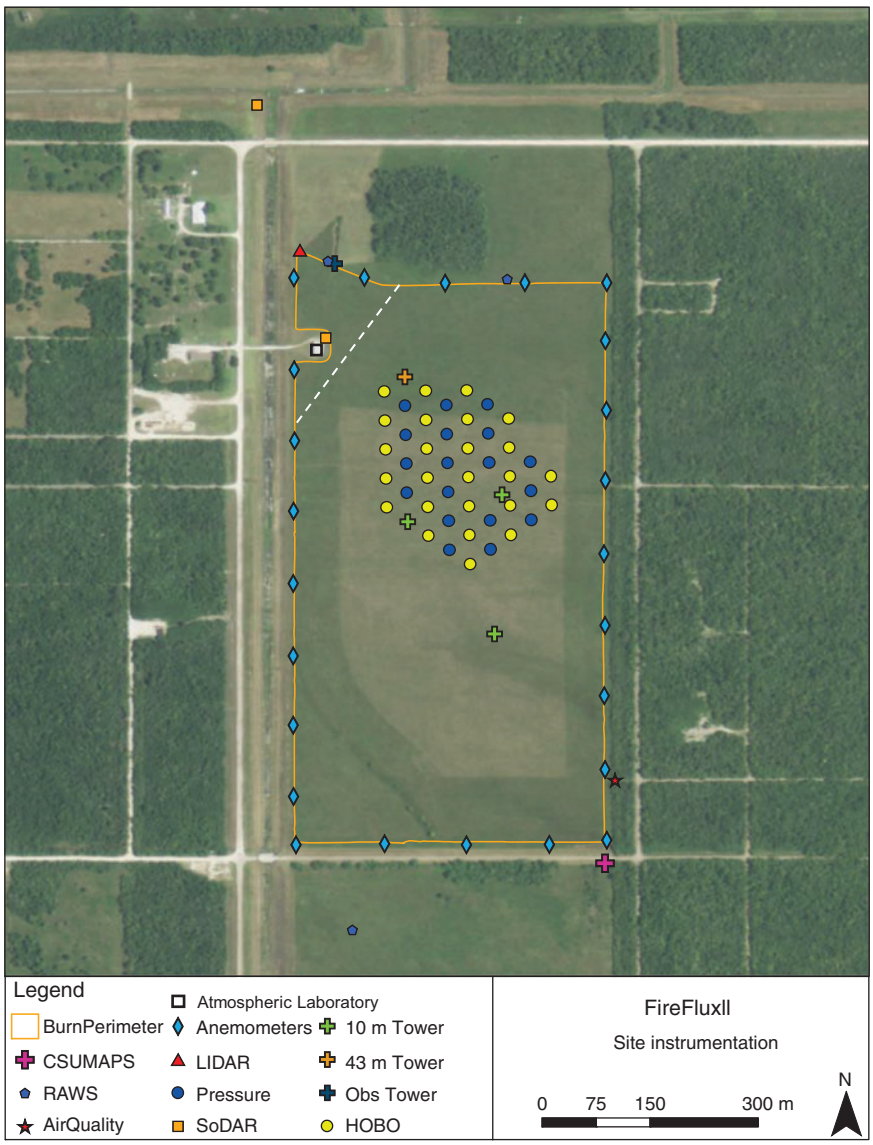

Fig. 1. Map of the final experimental design indicating instrument placement during FireFlux II (FF2), 30 January 2013. The ignition line is denoted by the white dashed line.

Laboratory (Fig. 1). The sodar next to the burn unit perimeter (Scintec, MFAS-64) collected wind speed and direction data between 20 and 600 m AGL at 10-m increments. The sodar located upwind of the burn unit collected wind speed and direction data between 10 and 200 m AGL at 5-m increments. A microwave profiler (Radiometrics, Corp., MP-3000A) was installed on the roof of the Atmospheric Laboratory and measured tropospheric profiles of temperature and relative humidity. Finally, a Doppler lidar (model Streamline 75, Halo Photonics, Ltd) was installed at the north-western corner of the burn unit; its field of view towards the 43-m tower is shown in Fig. 3*e*. The lidar conducted a combination of horizontal plan position indicator (PPI) scans and vertical range height indicator (RHI) scans in an L-pattern fashion (Fig. 4) in order to capture radial velocities and backscatter intensities horizontally across the fire front and vertically within the plume. The class 1M laser operates at a near-IR 1.5-μm wavelength, and has a 15-kHz pulse rate. The range of the laser for this experiment was 60 to 1000 m, with a range gate size of 18 m. The radial velocity measurements are accurate to within 0.038 m s^{-1}, with signal-to-noise ratios (SNR) exceeding 1.015SNR + 1. Figs 1 and 3*e* show the position of the lidar relative to the ignition line and the advancing fire front.

Three separate automated weather stations (AWS) were situated near the burn unit, measuring wind speed and direction, air temperature and relative humidity. One AWS was situated in the north-west corner of the unit. Using an RM Young 3D sonic anemometer, the station was designed to measure heat flux outside of the burn boundary. A second station was set up directly south of the burn unit, and was equipped with a temperature and relative humidity probe (CSI, CS215), as well as a propeller anemometer (RM Young, 5103). The final AWS

Table 1. Description of the atmospheric instrumentation used during FireFlux II (FF2)
AWS, automated weather stations; RH, relative humidity

Platform, instrument	Sensor type, manufacturer and model	Variables	Measurement height, range (m above ground level (AGL))	Sampling frequency (Hz)
Main tower (43 m)	3D sonic anemometers (RM Young 81000 and ATI SATI-3Sx)	u, v, w, T_s	5.8, 10.0, 20.0 and 43.0	10
	Type T thermocouples (Omega, Inc., 5SC-TT-40)	Temperature	Total of 11 mounted between 0.3 and 43	1
	Heat flux plate (Hukseflux, HFP01)	Soil heat flux	−0.08	1
	thermocouple probes (CSI TCAV)	Soil temperature	−0.03 and −0.08	1
	Pressure sensor (RM Young 61302V)	Pressure	3.0	1
	Dual band radiometer (Onset Computer, Corp.)	Radiative heat flux	5.8, 10.0	1
Short towers (10 m)	3D sonic anemometers (ATI, SATI-3Sx)	u, v, w, T_s	5.3	10
	Pressure sensor (RM Young)	Pressure	3.0	1
	Fuel temperature probe	Temperature	0.18	1
	Dual band radiometer (Onset Computer, Corp.)	Radiative heat flux	5.0	1
	Type E thermocouples (Omega, Inc., 5SC-EE-40)	Temperature	Total of nine mounted between 2 and 10 m, at 1-m intervals	1
	Pressure sensor (RM Young 61302V)	Pressure	3.0	1
	Heat flux radiometer (Medtherm 64 series)	Radiative heat flux	4.6	1
	Heat flux sensor (Hukseflux, SBG01)	Total heat flux	4.6	1
CSU-MAPS tower (32 m)	3D sonic anemometers (RM Young 81000)	u, v, w, T_s	9.0 and 31.0	10
	2D sonic anemometers	u, v	9.0, 16.5, 29.0 and 32.0	1
	Temperature/RH Probe (Campbell Scientific HMB45C) (Vaisala, HMP45C)	Temperature and relative humidity	9.0, 16.5, 29.0 and 32.0	1
Doppler lidar	Halo Photonics, Ltd, model Streamline 75	Backscatter intensity, radial velocity	60–9000, gate res.: 18	1
Microwave profiler	Radiometrics, Corp., MP-3000A	Temperature and humidity	20.0–9600.0	0.3
Doppler mini sodars	Atmospheric Research and Technology VT-1	u, v, w	15–200	10 min
	Scintec, MFAS-64	u, v, w	20–1000	10 min
Cup and vane anemometers	S-WCA-M003, Onset Computer Corp.	Wind speed and direction	3.3	0.33
HOBOs	Onset Computer Corp., U12-014	Flame temperature	0.0	1
Pressure sensors	Custom	Temperature and pressure	3.0	1
Flux AWS (north-west corner)	3D sonic anemometer (RM Young 81000)	u, v, w, T_s	1.5	20
Flux AWS (north-east corner)	3D sonic anemometer (Campbell Scientific, Inc. CSAT3)	u, v, w, T_s	1.5	10
	Net radiometer (Hukesflux, Inc. NR01)	Net radiation	1.25	1
AWS (southern edge of plot)	Temperature/RH Probe (Campbell Scientific, Inc. CS215)	Temperature and relative humidity	2	1
	Anemometer (Campbell Scientific, Inc. RM Young, 5103)	Wind speed and direction	1.5	1
Houston Mobile Air Quality Laboratory	Picarro, Inc., G2201-I	CH_4	2.5	1
	Picarro, Inc., G2201-I	CO_2	2.5	1
	MetCon Gmbh, 2-pi filter radiometer	jNO_2 (photolysis rate of NO_2)	2.5	1
	Thermo 49C	O_3	2.5	1
	Thermo, 48C-TLE	CO	2.5	1
	Air Quality Design, Inc.	NO/NOx	2.5	1
	Thermo, 42C-TL	NOy	2.5	1
	Tekran 2537A	Hg	2.5	1

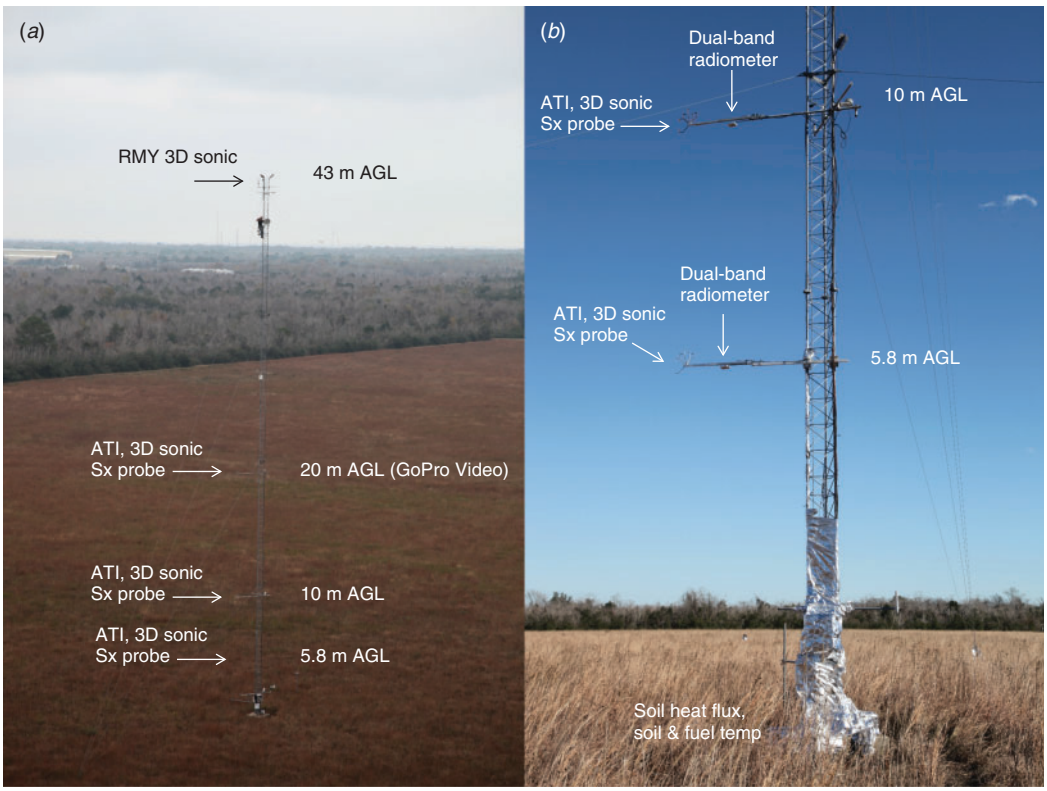

Fig. 2. Photos of the 43-m tower showing the arrangement of the sonic anemometers on the tower (*a*); and a close-up of the first 10 m of the tower (*b*) (ATI, Applied Technologies, Inc.).

was positioned on the northern edge of the burn unit, and was equipped with a 3D sonic anemometer (CSI, CSAT3) and a net radiometer (Hukseflux, Inc., NR01). Unfortunately, the battery that provided the power for this AWS was burned over during the experiment and the data collected were subsequently lost.

A Vaisala, Inc. radiosonde (RS92-GPS) was launched before the ignition from near the ignition site at 1424 Central Standard Time (CST) (Fig. 3*g*). The radiosonde recorded at 1 Hz temperature, dewpoint temperature, wind speed and direction, pressure, position and altitude.

In addition to the meteorological measurements, some plume chemistry species were sampled 2.5 m AGL directly downwind of the burn unit (Figs 1, 3*c* and 3*d*). The species included ozone (O_3), carbon dioxide (CO_2), methane (CH_4), carbon monoxide (CO), nitrogen oxide (NO), nitrogen dioxide (NO_2), oxidised forms of nitrogen (NO_y), and mercury (Hg). Aerosol concentrations ($PM_{2.5}$, particulate matter of 2.5 μm or less in diameter, and black carbon) were also measured, but the data were not recovered as the sensors were damaged during the experiment. In addition to the measurement of gases and aerosols, volatile and semi-volatile organic compounds (VOC, SVOC) emitted during the burn were analysed. Two Tenax TA sorbent tubes were used with a pump (Supelco®; 11.5 cm × 6-mm outer diameter and 4-mm inner diameter) to capture low- and medium-volatility organic compounds and were placed at two different heights (6 and 18 m) on the 43-m tower. Sampling was carried out during the fire at a flow-rate of 150 mL min^{-1}. The sorbent tubes were transferred to a freezing box before being analysed by automatic thermal desorption–gas chromatography/mass spectrometry (ATD-GC/MS).

Fire behaviour measurements

To measure the rate of spread of the fire front, two interspersed grids of HOBO temperature data loggers (Onset HOBO, U12–014) equipped with an Omega 20-gauge K-type thermocouple were placed just beneath the ground surface within the soil. Eighteen HOBOs were spaced 30 m apart, recording temperature just above the soil surface, at a rate of 1 Hz. An array of pressure sensors was also placed between the 43- and 10-m towers (Fig. 1). The pressure sensors, custom-built packages designed to collect pressure, internal temperature, external temperature, and GPS position data at 1 Hz, were installed 3 m AGL, and 30 m apart. Each sensor contained an aneroid barometer, GPS and a type-E thermocouple, and was mounted on a post and covered in protective fire-shielding material. This array was designed to provide fire front rate of spread estimates, as well as the measurement of pressure and temperature associated with the FFP.

Two additional sensor systems were deployed in the burn unit and embedded within the fuels to measure fire behaviour properties. The first type was a fire behaviour package (FBP) (Butler *et al.* 2016) that included a type-K thermocouple for flame temperature, a Schmidt–Boelter style radiometer (Medterm, Model 64–20T) that measured incident total and radiant energy flux, a custom-designed narrow-angle radiometer, and

two pressure-based flow sensors designed to measure horizontal and vertical gas flows associated with the fire front. All data from the FBP were recorded at 10 Hz using a CSI CR1000 datalogger. The second type of sensor package was a fire-proof box, which housed video cameras that recorded visible imagery of the flaming front as it approached the FBP. The suite of FBPs were placed near each tower in the burn unit (Figs 1 and 3*f*).

Videos and photographs were taken by a variety of cameras. A ground-based digital single-lens reflex (DSLR) camera (Canon 40D), positioned on the western edge of the unit, collected photos of the fire front and plume with a 1-Hz time lapse. A wide-angle Go-Pro Hero 3 camera was installed on the 40-m observation tower (Fig. 1) located at the north-west corner of the burn unit at a height of 40 m AGL, collecting video of the entire unit from an aboveground vantage point. A second Go-Pro Hero 3 was installed 20 m AGL on the 43-m tower, facing down, in order to capture the fire front passage through the instrument array. Finally, a helicopter flew ~400–500 m

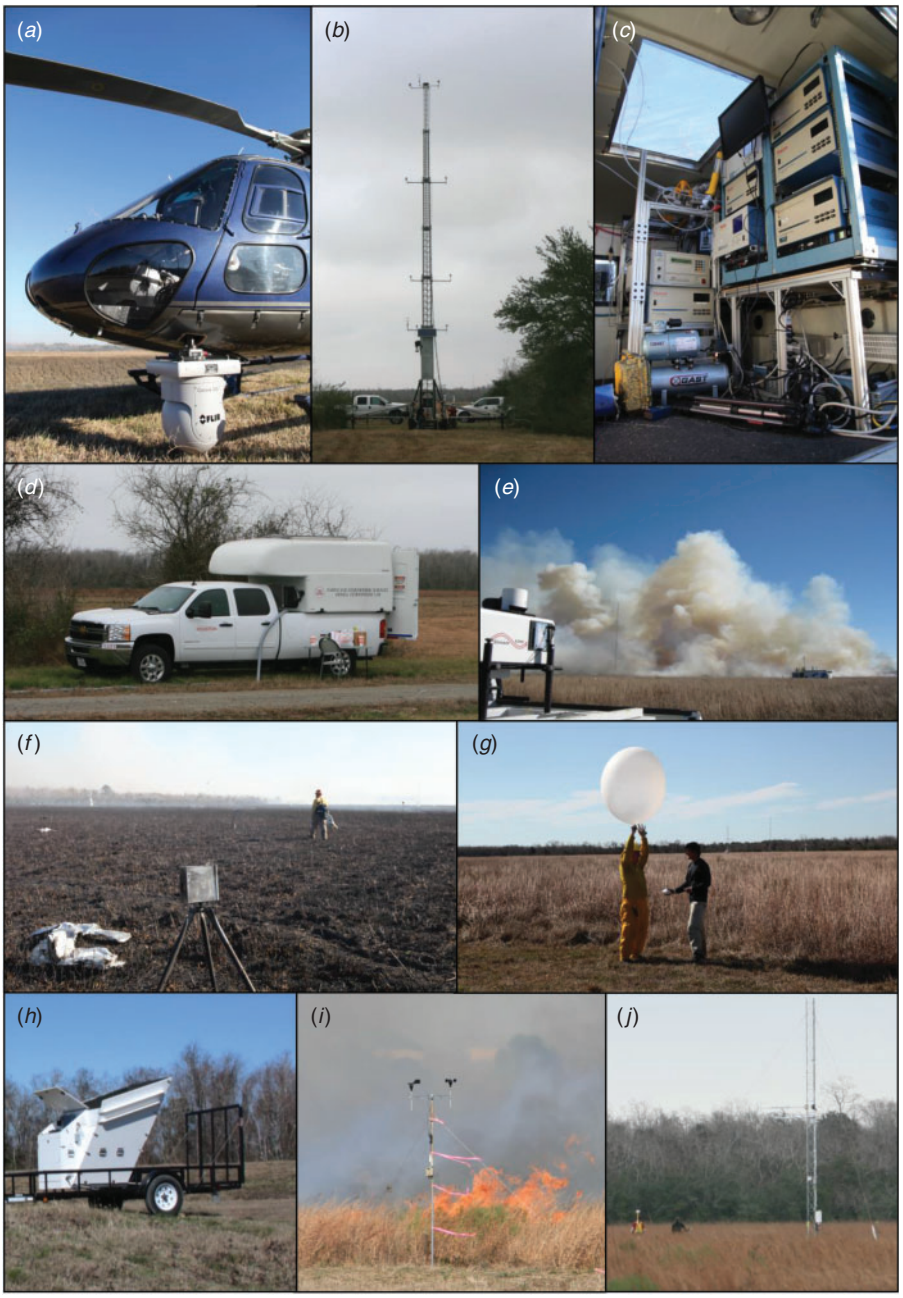

Fig. 3. (*a*) Helicopter-mounted FLIR camera and gimble system (Corona 350); (*b*) 32-m California State University Mobile Atmospheric Platform System (CSU-MAPS) tower; (*c*) mobile air quality instruments; (*d*) mobile air quality laboratory; (*e*) Doppler lidar; (*f*) fire behaviour video package; (*g*) radiosonde release; (*h*) ART VT-1 sodar; (*i*) cup anemometer on burn unit perimeter; (*j*) 10-m interior tower.

above the experimental site, capturing simultaneous visible and infrared video using a gyro-stabilised gimbal camera system (FLIR Systems, Inc., Corona 350; Fig. 3*a*). A photographer was also stationed in the helicopter, taking oblique aerial images using a Nikon DSLR camera. The helicopter flew in such a manner as to frame the entire burn unit, which made it necessary to increase altitude as the burn progressed. A second IR video camera (FLIR Systems, Inc., 640) was mounted on the observation tower 40 m AGL. Still visible images from the helicopter are presented in Fig. 5, whereas corresponding georectified temperature snapshots from the IR camera mounted on the 40-m observation tower are shown in Fig. 6. An additional FLIR 640 was pointed east and mounted 10 m AGL on the University of Houston Atmospheric Laboratory tower located ~25 m west of the ignition line.

Time synchronisation

In order to coordinate the timing of the fire with the time stamps of all the instruments, photos, videos and any other data collected, everything in the field needed to be time-synchronised. All cameras in the field were used to photograph an image of an atomic time clock. By comparing the photographed time with the timestamp on the camera image, a synchronisation could be calculated and applied to all images. All other timestamps on field computers and instruments were photographed, thereby allowing a simple time correction for each, based on the camera time. Although all data loggers were synchronised using GPS, similar photo comparisons were done as a failsafe.

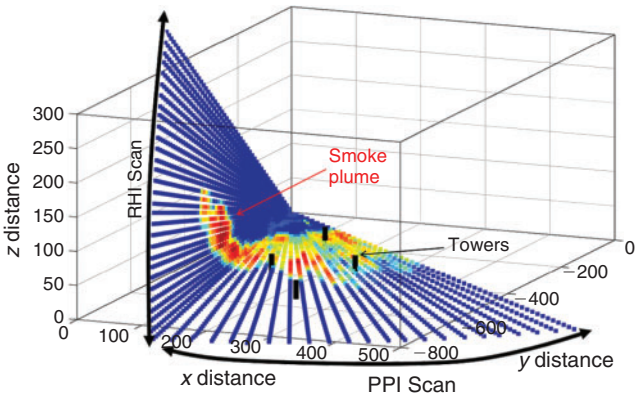

Fig. 4. Schematic of lidar scanning strategy. The L-pattern allowed horizontal plan position indicator (PPI) scans across the fire front and the vertical range height indicator (RHI) scan captured the plume structure along the flank of the fire. Data shown are lidar backscatter intensity.

Fuels sampling

The dominant fuel type in the experimental burn unit was tall grass, which consisted of cured native grasses including big bluestem (*Andropogon gerardi*), little bluestem (*Schizachyrium scoparium*) and long-spike tridens (*Tridens strictus*). Pre- and post-burn sampling were conducted on 4 January 2013 and 7 February 2013 respectively. The objective of the vegetation sampling was to characterise the structure and loading of combustible material within the burn unit. Twenty destructive clip plots (0.25 m^2) were established on a systematic grid within the burn unit at 25-m spacing. Clip plots were delineated by a 0.5 × 0.5-m PVC square. All vegetation within each plot was cut and separated into four categories: upper layer grass, lower layer grass, forb and shrub. The boundary between the two grass layers reflects the visual assessment of the maximum continuous distribution of biomass, or centre of mass height.

All vegetation samples were labelled, checked, boxed and shipped to the USFS's Pacific Northwest Wildland Fire Sciences Laboratory in Seattle, WA, for processing. Samples were oven-dried at 70°C until a constant weight was achieved, which was typically 48 h. Net dry weights were recorded, entered into data templates, and checked twice by different technicians to ensure accuracy. Fuel loading from vegetation data was determined using a macros-based *Excel* spreadsheet.

Post-burn fuel sampling was primarily conducted in areas wherein an uninterrupted head fire was observed during the prescribed burn. The identification of areas that received

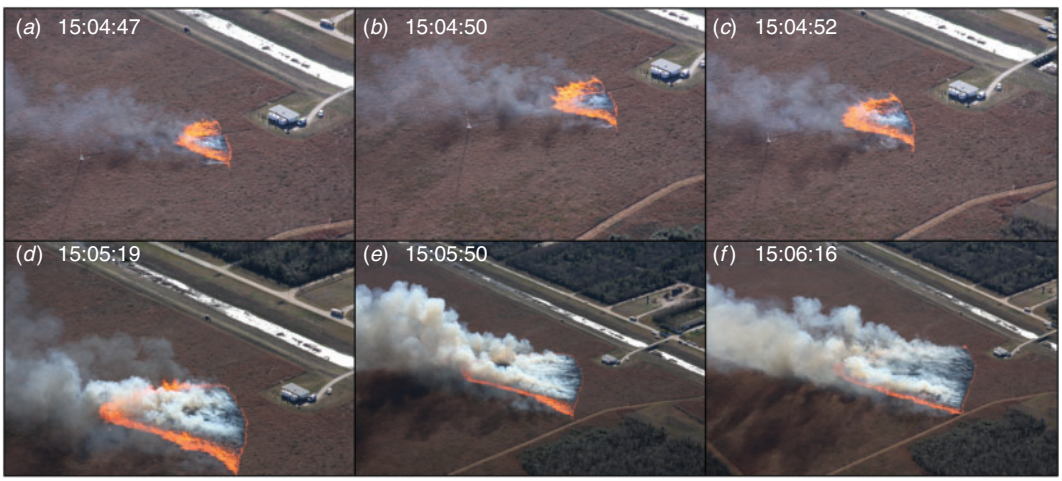

Fig. 5. Photographic time series of fire front positions and fire shape. Times are HH:MM:SS (Central Standard Time, CST).

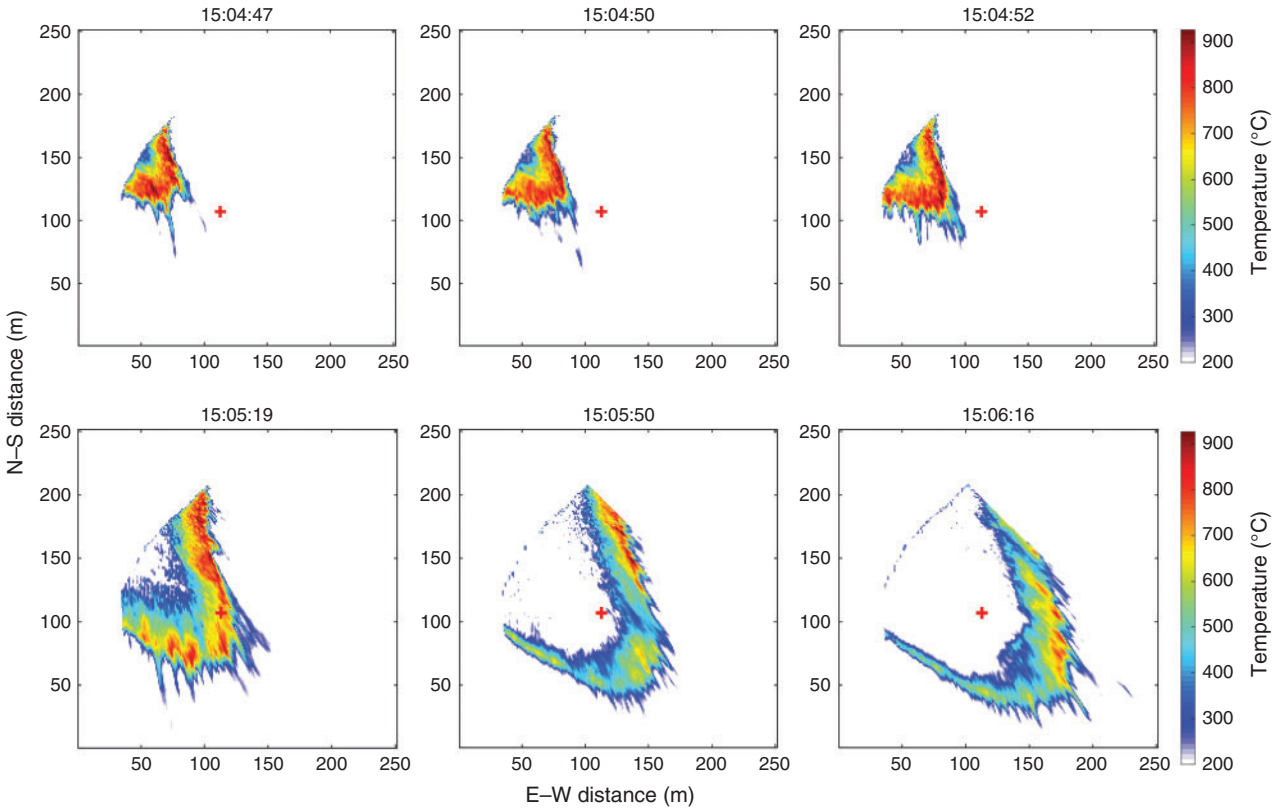

Fig. 6. Series of geo-referenced infrared (IR) temperature (°C) observations from the 40-m observation tower located north of the unit boundary. Red cross shows location of the 43-m tower inside of the burn unit (see Fig. 1 for locations of all towers). Times are HH:MM:SS (Central Standard Time, CST).

uninterrupted head fire was corroborated by burn operations personnel and video. Forty-six destructive clip plots (0.25 m^2) were established on a systematic grid within the burn unit at 25-m spacing. Of the 46 destructive post-fire clip plots, 14 were installed in areas wherein a flanking fire was observed. The purpose of the post-burn plots was to quantify loading by vegetation life form for the post-burn environment. Biomass consumption for each vegetation category was determined by subtracting pre- from post-burn fuel loads.

Fuel moisture sampling was conducted within 30 min of ignition. Samples ($n > 5$) of each vegetation category were collected outside the perimeter of each burn unit. All moisture samples were sealed and the net green or wet weights were measured as soon as possible in the field, but generally within 6 h of ignition. Moisture samples were then checked and processed onsite at the HCC. Samples were oven-dried at 70°C for 48 h and moisture contents (%) were determined using a macros-based *Excel* spreadsheet.

Surface-area-to-volume (SAV) sampling was also conducted inside the perimeter of the burn unit before ignition. A total of 12 additional destructive clip plots (0.0625 m^2) were established on a systematic grid during pre-burn sampling to describe the fuel surface area available for heat and mass transfer. Clip plots were defined by a 0.25 × 0.25-m PVC square (Fig. 7). The maximum height of vegetation within the plot was measured to the nearest 0.5 cm before clipping. The boundary between the upper and lower grass layers was determined from dozens of measurements of the visual estimate of centre of mass for the species. This value (30 cm) was fixed to ensure sampling was conducted in a consistent and replicable manner by field technicians. Biomass clipped above 30 cm was classified as the upper layer, and biomass collected below 30 cm was classified as the lower layer. Samples were further sorted into like-size and shape categories. These categories included large cylinders, small cylinders, large blades, small blades and seed heads. Shape categories and size classifications varied slightly by species. Once sorted, geometric features of a subset of eight specimens within each category were measured with calipers to the nearest 0.01 mm to calculate the surface area (mm^2) and volume (mm^3) of each specimen. In categories defined as 'blades,' one total length measurement, four width measurements and four depth measurements were recorded for each specimen. In categories defined as cylinders, one total length measurement and four diameter measurements were recorded for each specimen. Owing to the small size of seeds, only one width (major axis), depth (minor axis) and length measurement was recorded for each specimen. Surface area and volume for seeds were approximated as ellipsoids. Surface area and volume measurements for grass blades were then approximated as rectangular prisms. Cylinder values were approximated using an average of diameter measurements. Each of the eight specimens per category was then weighed to 0.001 g. For each plot,

Fig. 7. Photograph of the fuels and the 0.25 × 0.25-m clip plot.

all biomass within a given category was oven-dried at 70°C for 48 h. The measured proportion of specimen mass to category mass was then used to approximate the total number of specimens in each category. Surface area and volume calculations were then scaled up from the specimen level to the category level. Table 2 lists the fuel loading characteristics. The unit average fuel loading was 0.64 kg m^2 with minimum and maximum of 0.41 kg m^2 and of 0.81 kg m^2, respectively. Most of the mass or loading was located in the lower grass layer. The average fuel moisture content of all vegetation types sampled on the morning of the burn was 14.2% (Table 3).

Synoptic weather conditions

The experiment was conducted in the midst of Texas' wildfire season and was initially scheduled in anticipation of a winter-time cold front passing through coastal Texas that would likely lead to dry, north winds. Forecasts on 26 January 2013 indicated that a cold frontal passage would occur during the night of 29 January, but would be followed by a post-frontal wind from the north-west, instead of a north wind.

The North American Regional Reanalysis (NARR) was used to analyse the synoptic weather conditions that occurred during the experimental period. As shown in Fig. 8, a trough moved through Texas the day before the burn. A cold front was associated with the passing trough, which is illustrated by the surface dew point shading in Fig. 8. At time, T – 18 h (2100 CST 29 January), the trough axis was located over the Texas Panhandle, with the cold front approaching the experimental

Table 2. Fuel loading characteristics (kg m^{-2})

Vegetation Type	Mean	s.d.	s.e.	Minimum	Maximum	95% CI
Grass lower layer	0.56	0.15	0.03	0.30	0.81	0.07
Grass upper layer	0.02	0.03	0.01	0.00	0.12	0.01
Forb	0.03	0.03	0.01	0.00	0.13	0.01
Shrub	0.04	0.11	0.02	0.00	0.36	0.05
Total	0.64	0.15	0.03	0.41	1.03	0.07

site (grey star in Fig. 8). At the time of ignition (Fig. 8, T = 0; ~1500 CST), the trough axis was located over Houston. The cold front passage occurred 16 h before time of ignition. Surface observations at the burn unit showed the frontal passage occurred at ~2200 CST 29 January (Fig. 9). The Doppler sodar profiles (Fig. 10) show that the pre-frontal wind profiles were southerly from 25 to 400 m AGL, and transitioned to SSW from 150 to 400 m AGL. After frontal passage, the winds were north–north-westerly between 25 and 400 m AGL. Wind profiles remained nearly uniform with height after frontal passage, but transitioned to more north-westerly near the time of ignition.

The sounding data are shown as a skew-T diagram in Fig. 11. The winds were north-westerly and extended through the boundary layer, which extended to 780 hPa (2.1 km AGL) as indicated from the neutral temperature profile. The wind direction transitioned from north-westerly to westerly flow above the boundary layer, and remained nearly uniform through the remainder of the profile.

On the night before the burning on 29 January 2013, the predicted cold front moved through the region and ~0.23 cm of rain fell around midnight, bringing January's rain total for the site to 7.6 cm. The temperature dropped from a maximum of 21°C on 29 January to 16°C at the time of the experiment on 30 January. The frontal passage brought about a wind shift from 180° to 315°, an increase in surface wind speeds from 6–8 to 10–12 m s^{-1}, and wind gusts in excess of 20 m s^{-1}. Fig. 9 shows the wind speed and direction at the time of the frontal passage. At the time of ignition, skies were clear, the temperature was 15.6°C, the relative humidity was 23%, and surface winds remained west–north-westerly throughout the burn. These conditions led the National Weather Service (NWS) to issue a Red Flag Warning (weather that can lead to extreme burning conditions; https://w1.weather.gov/glossary/index.php?letter=r;accessed 12 March 2019) for the region, which overlapped with the timing of the proposed burning. In addition, there was a regional burn ban in place.

Ignition procedure

The fire was ignited at 15:04:08 CST as a line fire extending along the north-west corner of the burn unit. Two firefighters, each with a hand-held drip torch, walked ~100 m in opposite directions from the centre of the ignition line to the edge of the unit boundaries. The northern branch of the ignition took ~110 s to complete while the southern branch was paused for ~20 s until it was continued to the edge of the burn plot, which took an additional 90 s owing to the drip torch being blown out by the wind. The decision to pause the southern branch of the ignition was made by the ignition team member for unknown reasons.

Table 3. Fuel moisture values per sample type taken 30 min before ignition, 30 January 2013

Vegetation type	Sample size (***n***)	Mean (%)	Median (%)	Confidence level (95%)	s.e.	s.d.
Grass upper layer	5	8.49	9.05	1.01	0.52	1.15
Grass lower layer	10	18.14	17.17	2.00	1.02	3.22
Forb	5	16.07	9.56	12.77	6.51	14.57

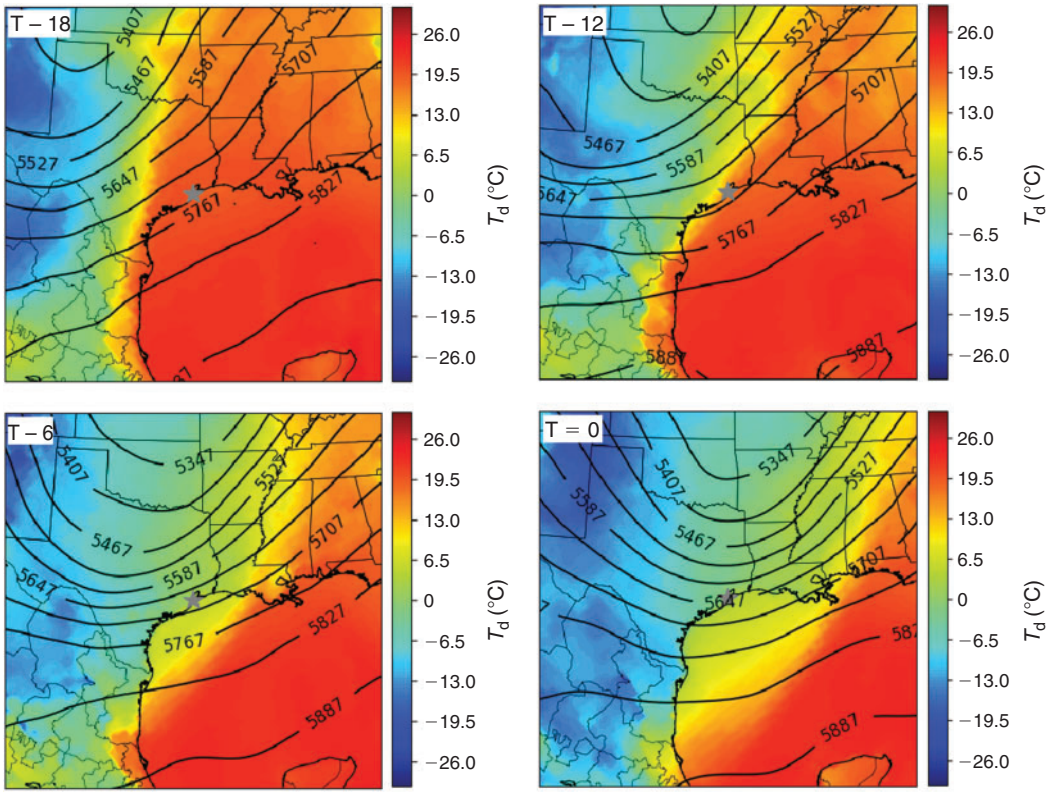

Fig. 8. North American Regional Reanalysis (NARR) 500-hPa geopotential height (contours) and surface dew point, T_d (shading). The geopotential height contours are in increments of 60 geopotential m. These data show the progression of the trough and cold front (dewpoint boundary) across Texas in the 18 h preceding ignition where T –18 is 2100 CST (Central Standard Time) on 29 Jan 2013, T – 12 is 0300 CST on 30 Jan, T – 6 is 0900 CST on 30 Jan, and T = 0 is 1500 CST on 30 Jan.

The fire spread resulted in a parabolic fire line driven into the instrument array by the ambient winds.

Coupled modelling for experimental design

One of the key goals of the experiment was to provide *in situ* observations of the winds and temperature above the propagating fire front. In order to accomplish this, the sensors were originally arranged in a large cross-pattern oriented in north–south direction, with its north defined by the location of the 43-m tower (Fig. 12*a*). This configuration was designed for the fire spread to be driven under a north wind that would generate a parabolic fire front propagating southward through the burn unit. In this configuration, the head fire was expected to impinge on the 43-m tower and one of the short 10-m towers, while the flanks would be sampled by the two most southern 10-m towers.

As the proposed date for the burning approached, the chances of a northerly surface wind were gradually diminishing. All weather forecasts issued within 1 week of the proposed burn date were indicating north-west or west–north-west winds, which would result in a very narrow fire front and its head missing all the short towers and most of the ground sensors indicated in Fig. 12*a*. In order to assess how the fire would propagate under the forecast westerly winds, a set of preliminary coupled fire–atmosphere model simulations, WRF-SFIRE (Mandel *et al.* 2011), were performed. The model was configured in an idealised mode, similarly to the run performed for the original FireFlux experiment (see Kochanski *et al.* 2013 and Table 4 for details) and the vertical temperature and moisture profiles were

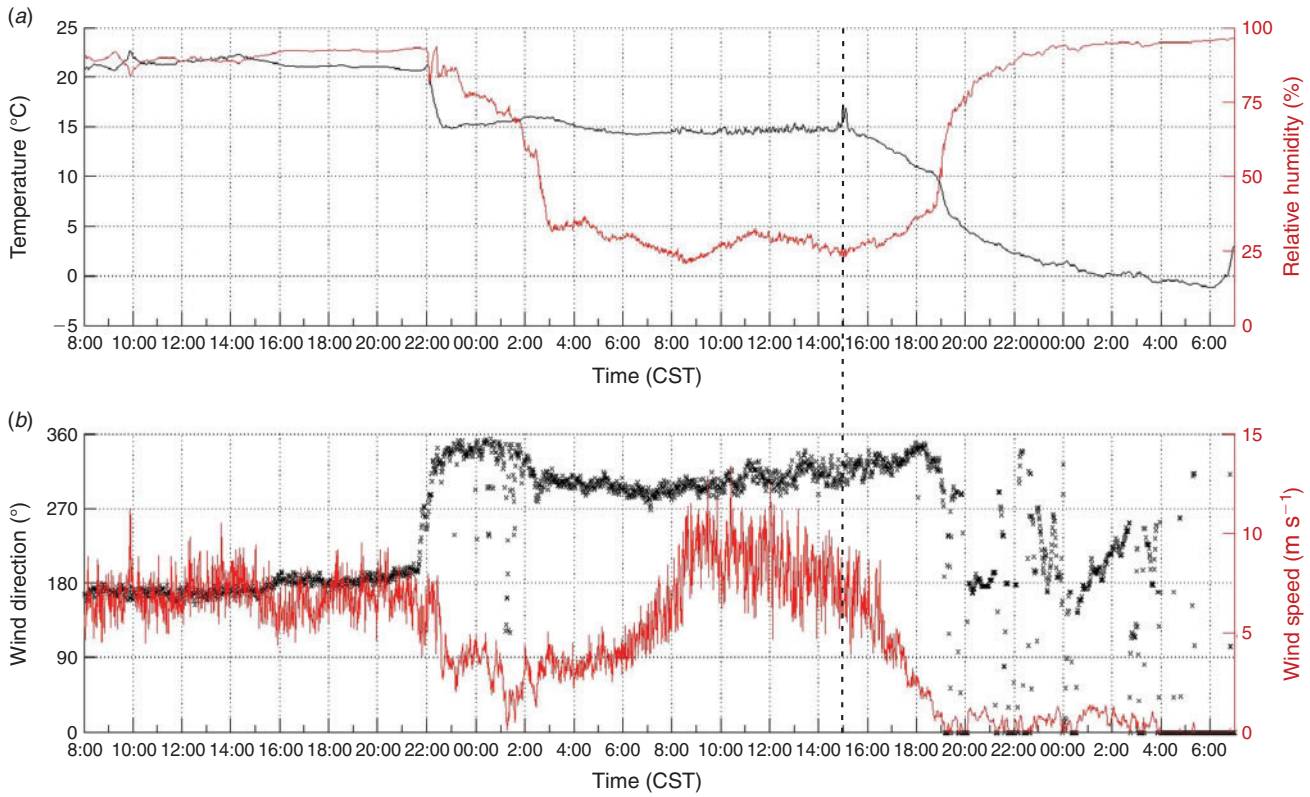

Fig. 9. Time series of temperature, relative humidity (*a*), surface wind speed and wind direction (*b*) for 29–30 January 2013 taken from the University of Houston Atmospheric Laboratory located on the western edge of the burn unit (Fig. 1, sodar location). Ignition time is marked by the vertical dashed line.

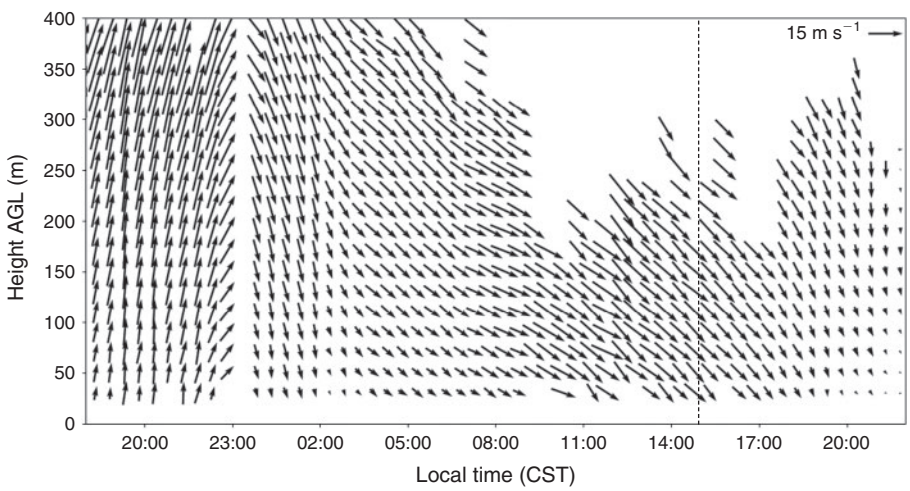

Fig. 10. Time–height plot of vertical wind profiles obtained from the Doppler sodar located next to the burn unit, near the University of Houston Atmospheric Laboratory (Fig. 1). Data are from 29–30 January 2013. Dashed line indicates time of ignition.

initialised using the observations from the previous FireFlux experiment in 2006. The wind field, however, was initialised with two neutral-log profiles with friction velocities of 0.68 and 0.93 m s^{-1} and a surface roughness length of 0.15 m. These two profiles were designed to provide 10-m winds of 7 and 8.5 m s^{-1} respectively. The wind direction was set to 290°, 310° and 330° in order to cover a range of forecast wind directions. All the test simulations were performed with two walking ignition lines starting from a common point in the middle of the northern unit and extending east and west. These simulations indicated that

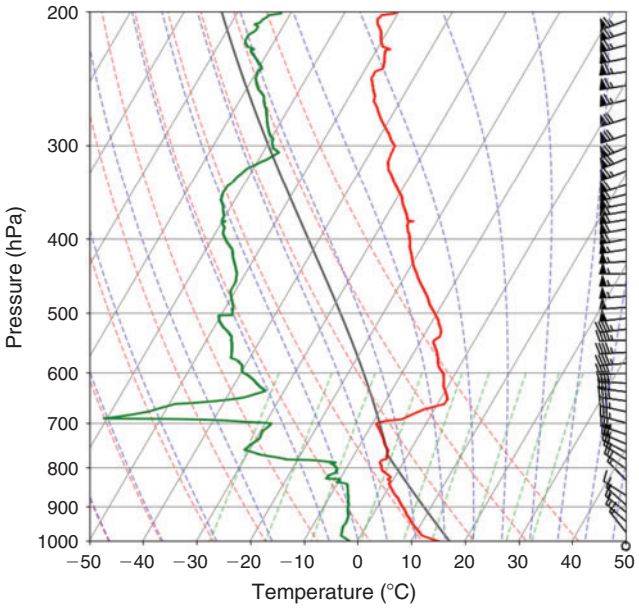

Fig. 11. Radiosonde sounding taken at 1424 CST (Central Standard Time) just before ignition on 30 January 2013. The red line represents the temperature and the green line the dew point.

the head fire would barely strike the 43-m tower and miss most of the ground sensors and all the short towers (see the red fill of Fig. 12*b*). In light of these simulations, it became clear that the original experimental design had to be modified. The original ignition line was modified in order to extend the width of the fire front and maximise the sampling of the fire-induced circulations near the head and the flanks of the fire. The final simulated ignition was conducted using two segments, oriented normal to the expected wind direction of 290° and 320°, forming a 150° wide 'V' shape as shown in Fig. 12*b*. The new ignition procedure was implemented in the model and was executed again for the wind direction of 310°. Based on this new fire simulation (light blue fill in Fig. 12*b*), the decision was made to relocate the surface sensors as well as one of the 10-m towers. The main goal was to maximise probability of having two towers sampling the wind and temperatures associated with the head fire and two towers sampling the winds and temperatures near the flanks. Additionally, this would enable determining the local rate of spread from *in situ* surface sensors independently from the IR observations.

Preliminary results

Observations of fire behaviour

As mentioned in the previous section, fire behaviour was monitored using three IR cameras (two mounted on towers and a third mounted in a helicopter), ground-based temperature loggers, and *in situ* visible video cameras and heat flux radiometers. The helicopter IR camera provided both visible and IR images of the burn unit (Fig. 5). As shown in Fig. 5, the fire front is shown progressing from the ignition line towards the 43-m tower as a parabolic shaped fire front (Figs 5*a–f*). The IR camera looking east from the air quality laboratory 10 m AGL provided only a limited low-elevation rear and side view of the fire. The IR camera mounted atop the 40-m observation tower proved to be the best source of fire behaviour imagery as it recorded video covering most of the burn unit. The 43-m tower, with its three anchor lines, and six additional points to the north, were used as reference points for georectification. The georeferenced IR images of recorded temperatures are shown in Fig. 6. The ignition line oriented approximately normal to the mean wind direction resulted in an almost symmetrical parabolic fire front shape, with the maximum temperatures reaching 900°C. The average head-fire rate of spread over the first 90 s of the fire progression, presented in Fig. 6, was ~1.6 m s^{-1}. The flank-fire propagation was estimated between 0.8 and 0.96 m s^{-1}. The IR images provide a good overview of the fire front shape and its time evolution. However, the exact position of the head-fire front cannot be easily derived based on these IR images. The oblique view angle and significant flame lengths (up to 5 m) limited precise estimation of the location of the fire front on the ground, especially at large distances from the observation tower. For that reason, the IR data have been complemented by the rate of spread and fire isochrones derived from the surface HOBO sensors recording soil-surface temperatures via thermocouples (Fig. 13). Additionally, fire front behaviour was interpolated from the GoPro (NW tower camera), using *OpenCV Library* (Bradski and Kaehler 2008) to correct for lens distortion, filter fire pixels and orthorectify the resulting images. These data were also compared with simulations of the experiment using ForeFire-MesoNH (Filippi *et al.* 2013).

The HOBO thermocouples were deployed in a rectangular array, which allowed calculating the speed and direction of the fire front for each triangle of thermocouples (two triangles per rectangle) from the FFP times at the thermocouples (Fig. 13). The FFP time was defined as the time when the temperature first reached 400°C. This temperature was chosen as a consistent threshold observed at each sensor. The maximum temperatures recorded ranged from 504 to 728°C, with an average of 613°C, and were reached 10 s after FFP on average.

The fire front speed and direction were calculated for each triangle from the fire front passage times at the triangle vertices (Fig. 13) using the method of Simard *et al.* (1984). The method is most accurate when the fire front within the triangle is a straight line. For a given number of thermocouples (and triangles), there is a trade-off between accuracy, which is greater for small triangles, and areal coverage, which is greater for large triangles. In addition to the fire front motion vectors, Fig. 13 displays isochrones of the fire front at 10-s intervals. The combination of the vectors and isochrones clearly shows the head fire propagated in the same direction as the surface wind towards the south-east at rates of 1.2 to 2.5 m s^{-1}, and the flanking fire propagated more slowly towards the south-west at speeds of 0.5 to 1.5 m s^{-1}, with a median speed of 0.8 m s^{-1}.

Observations of fire–atmosphere interactions

One of the main goals of the experiment was to simultaneously measure the near-surface atmosphere and fire behaviour to better understand fire–atmosphere interactions and their role in fire spread. The instrumentation array allowed winds and temperatures to be measured during the FFP. Fig. 14 shows a time–height

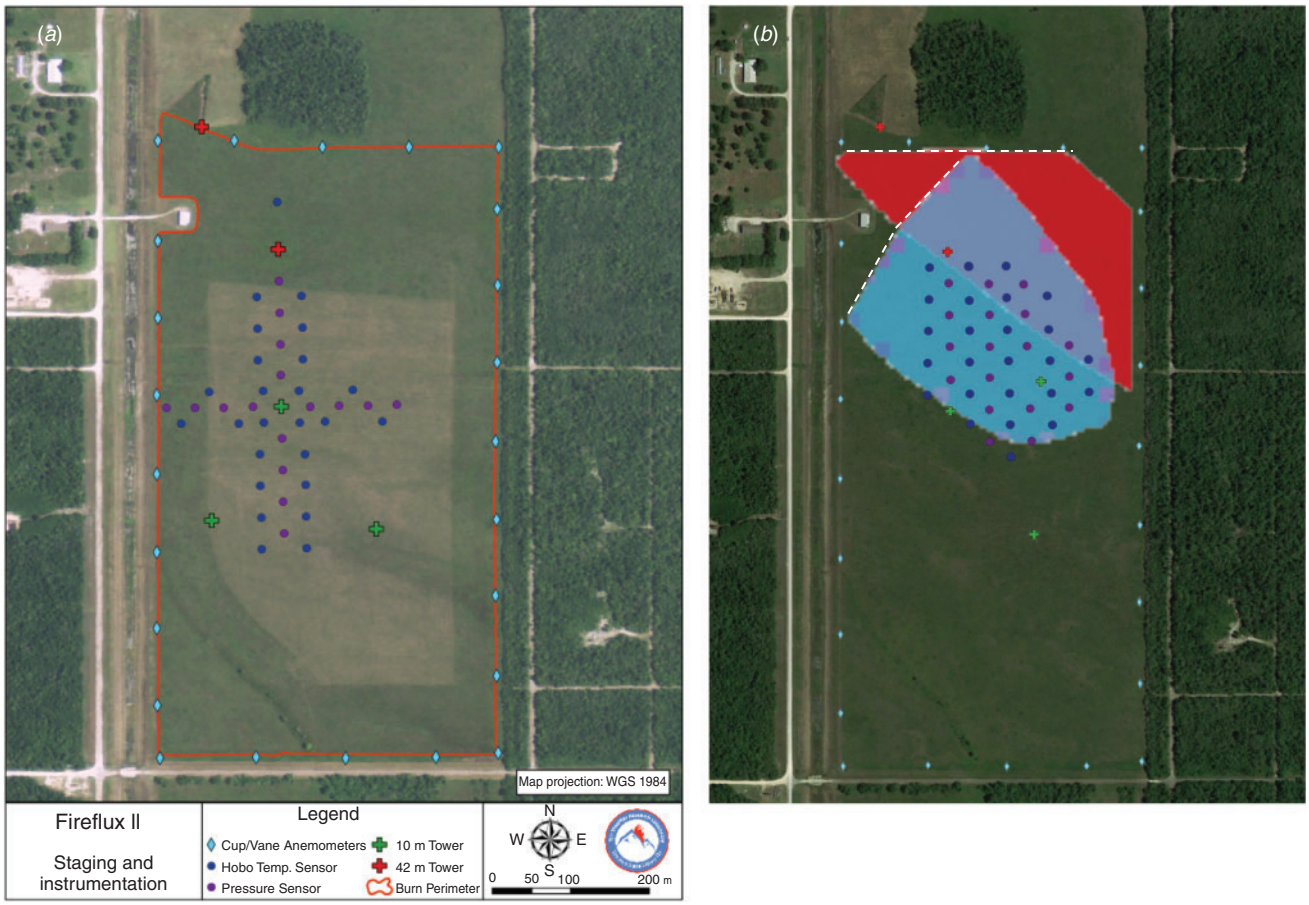

Fig. 12. (*a*) Experimental design plan initially laid out within the burn unit. (*b*) Modified experimental design plan, showing the WRF-SFIRE simulated fire area (colour fills) 540 s after the ignitions (white dashed lines). Red – simulation with the original E–W oriented ignition line, and blue simulation with the modified diagonally oriented V-shape ignition line. Both simulations performed for wind direction of 310° and 10 m wind speed of 8.5 m s^{-1}.

Table 4. WRF-SFIRE model parameters

Simulation type	LES (Large Eddy Simulation)
Horizontal domain size	1000 × 1600 m
Atmospheric mesh	160 × 100 × 80
Horizontal resolution (atmospheric mesh)	10 m
Model top	1200 m
Vertical resolution (atmospheric mesh)	From 2 m at the surface to 33.75 m at the model top
Fire mesh	3200 × 2000
Horizontal resolution (fire mesh)	0.5 m
Simulation length	15 min
Time step	0.02 s
Subgrid scale closure	1.5 TKE (Turbulence Kinetic Energy)
Lateral boundary conditions	Open
Surface layer physics	Monin–Obukhov similarity theory (sf_sfclay_phys = 1)
Land surface model	SLAB 5-layer MM5 model (sf surface_physics = 1)
Length of the western ignition line	170 m
Thickness of the ignition line	1 m
Heat extinction depth	6 m
Fuel depth	1.35 m
Ground fuel moisture	18%
Fuel load	1.08 kg m^{-2}
Fuel type of the burnt area	3 (tall grass)
Inflow wind profile	Logarithmic with $U^* = 0.68$ m s^{-1} and $z_0 = 0.15$ m s^{-1}
Inflow wind direction	310 deg

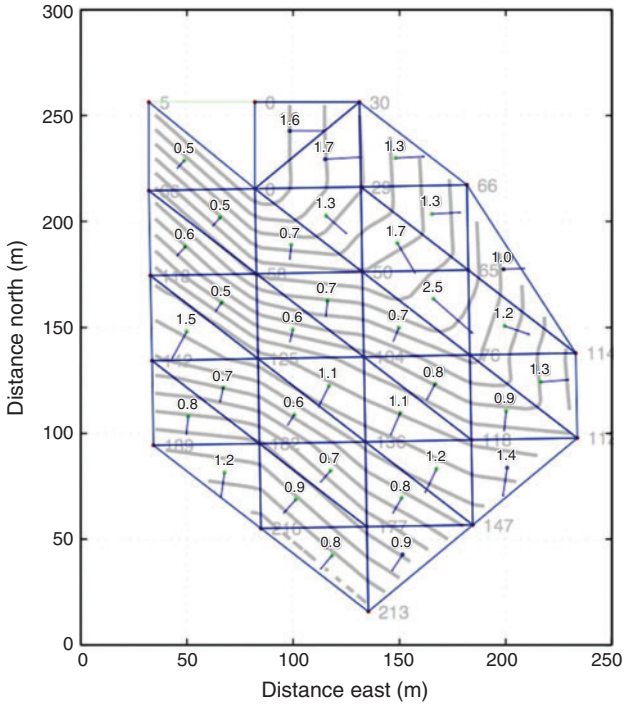

Fig. 13. Rate of spread vector calculation made from 25 HOBO ground thermocouples: arrival times (s) at each HOBO, isochrones at 10-s intervals, ROS (rate of spread) vectors and ROS speed.

plot of winds, temperatures and pressure from the 43-m tower during the FFP. The ambient winds were blowing from the northwest at each level (5.8, 10, 20 m AGL) before FFP. The plume height at this point during the fire spread was shallow, only 35 m AGL as indicated by the temperature contours in Fig. 14. The maximum plume temperature measured was ~300°C and occurred at 15:05:30 CST and was associated with FFP. This temperature maximum was located near the surface ~1.5 m AGL and represents the hot combustion gases, which were being advected by the surface winds. Corresponding to this temperature maximum was a maximum in negative surface pressure perturbation of approximately −0.3 hPa. This region of lower pressure was located at and just downwind of the fire front and was associated with the hot gases of the flaming zone. This low pressure caused the surface winds to accelerate and flow through and ahead of the fire front from upwind, advecting ignition temperature gases to the unburned fuels. This process was previously observed by Clements and Seto (2015). What is also interesting is the absence of flow modification ahead of the fire front. There was a slight shift in wind direction 30 s before FFP, from north-westerly to a more westerly direction (at 15:05:00 CST), most noticeably at the 6-m level and less so aloft, although the winds at all levels do indicate a shift in direction. This lack of flow modification was most likely caused by the strong ambient winds, limiting development of any fire-induced circulations. Winds after the FFP actually weakened slightly as the pressure perturbation decreased behind the fire front.

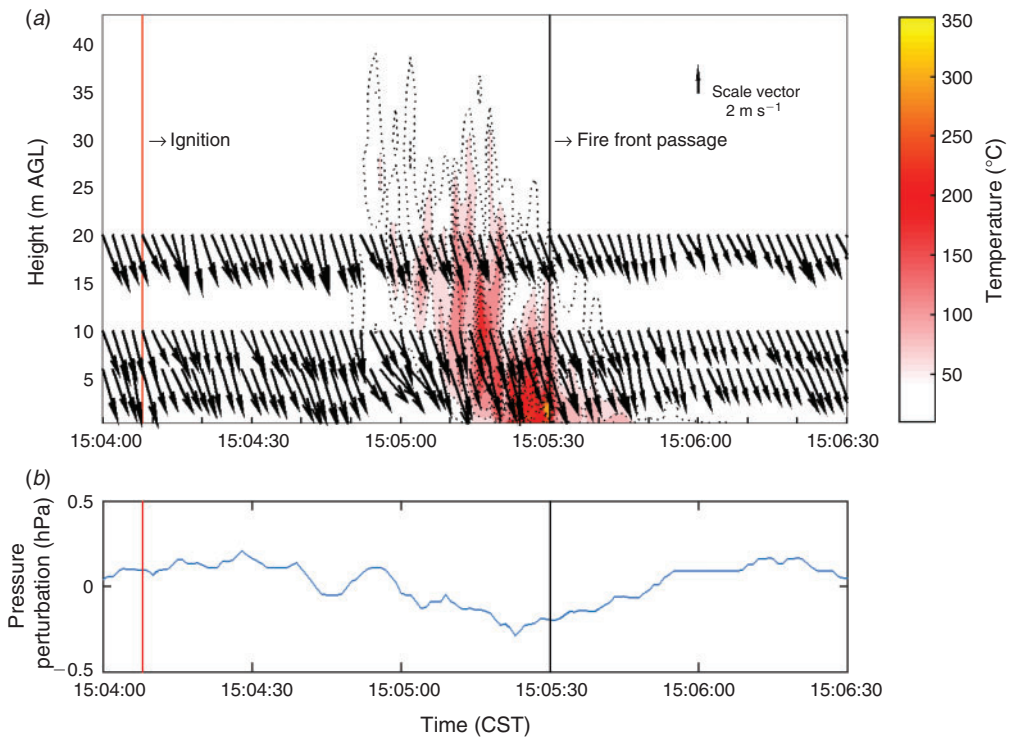

Fig. 14. Time height plot of thermodynamic plume structure, winds and surface pressure perturbation, measured at the 43-m tower. (*a*) Thermocouple temperatures (shading and contours) and horizontal wind vectors 5.8, 10 and 20 m AGL; and (*b*) the pressure perturbation, p′ time series is shown in the lower panel. The vertical red line is the time of ignition and the black vertical line is the time of fire front passage.

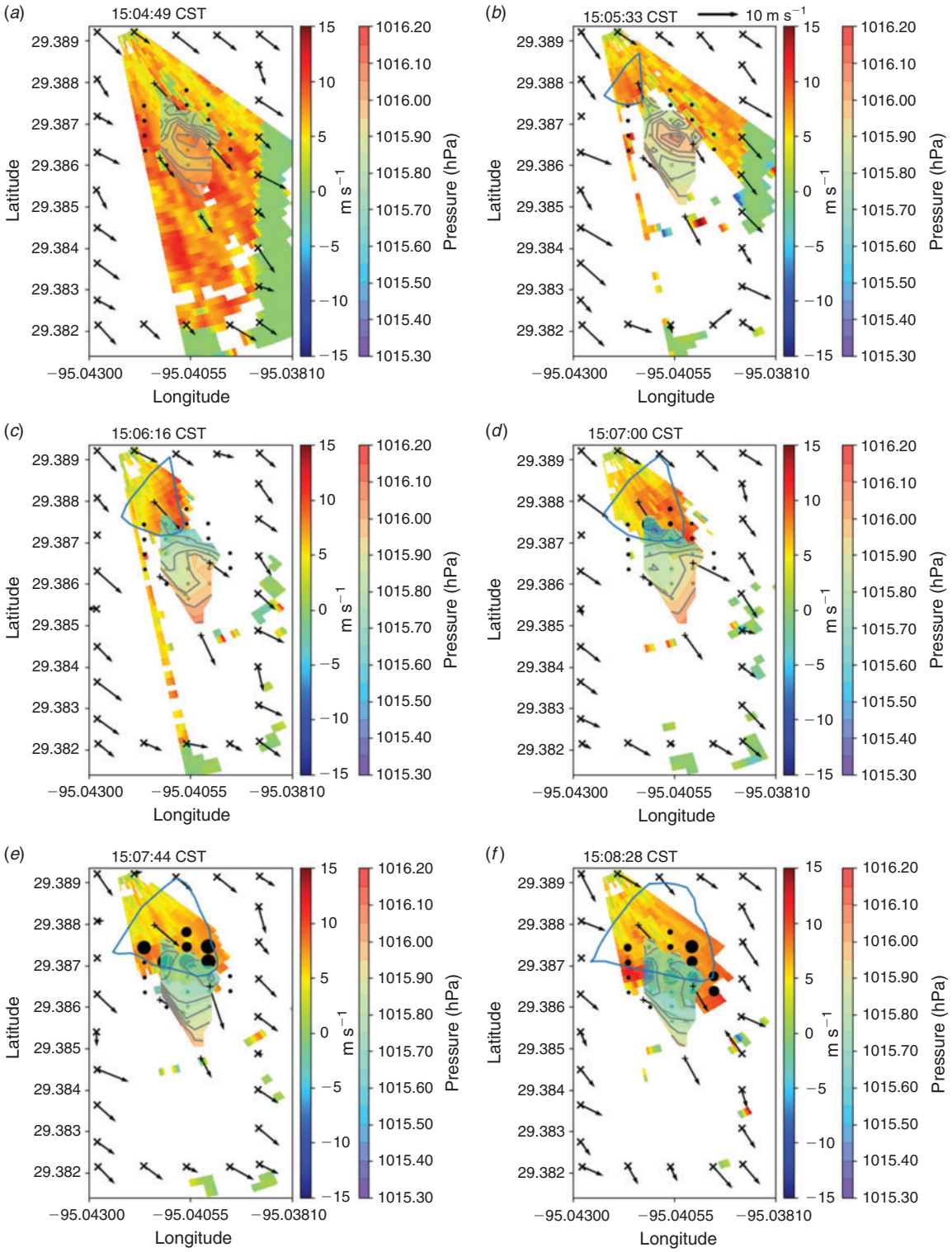

Fig. 15. Composite of surface winds from tower and anemometer arrays (vectors), Doppler lidar radial velocities (shading), 3-m barometric surface pressure (shading and contours) and soil surface temperature (black dots; larger size indicates higher temperature). The estimated fire perimeter (indicated by single blue outline) was derived from infrared temperature data obtained from the observation tower.

Further analysis of the spatial distribution of surface winds and surface pressure as they relate to the fire front position is shown in Fig. 15, which shows a composite of Doppler radial velocities from the lidar and surface winds measured by the anemometer and tower arrays. The key feature is the increased velocity observed at the fire front (darker red shading) and increased vector lengths (Fig. 15*d–e*). However, the increased wind velocity downwind of the fire front is somewhat intermittent and not continuous across the fire front. For example, the winds at the south-west interior tower actually decrease somewhat at 15:07:01 and 15:07:45 CST (Fig. 15*e–f*). This may be caused by the local pressure gradient that is directed from higher pressure to lower pressure, from downwind of the fire front back towards the fire. The strong ambient winds overcame this local pressure gradient and so a wind reversal was not observed, contrary to what would be expected during grass fires of similar scale (Clements *et al.* 2007; Clements and Seto 2015). One observation is that the local surface pressure field developed quickly and lower surface pressure was observed to occur in the vicinity of the fire front, both just downwind of it and within the flame zone (Fig. 15*c*). This pressure field developed in response to the hot gases of the combustion zone and the plume. The pressure decrease, which formed at the base of the convective column, produced an indraft into the column strengthening winds at the fire front and accelerating the fire spread. This phenomenon has been noted previously during a small-scale field experiment (Clements and Seto 2015), and in the laboratory (Finney *et al.* 2015) where the buoyancy-driven instabilities cause circulations to develop that cause flame peaks and troughs to develop in response to the resulting circulations (Finney *et al.* 2015). It is at the trough where the air behind the fire front penetrates through the fire front and spreads the flames towards the unburned fuels. This phenomenon has been described in detail by Finney *et al.* (2015) who also showed these structures were present in other field-based experimental fires (e.g. ICFME). Our observations provide further evidence that this phenomenon does occur in grass fires associated with strong surface winds.

Summary and future work

The FF2 experiment was conducted to better understand the micrometeorological aspects of fire spread. The experimental design was guided by the use of a coupled fire–atmosphere model that predicted the fire spread in advance. This information was used to relocate instrument towers just ahead of the burn date. The experiment was conducted under a regional burn ban and National Weather Service Red Flag Warning conditions, which highlights the uniqueness of the experimental conditions. Results show that as the ignition began, a negative surface pressure perturbation developed and strengthened as the fire front and plume developed and spread through the instrumentation array. The winds measured by both the Doppler lidar and *in situ* towers showed that there was an increase in wind velocity at the fire front, but also that winds downwind of the front did not reverse into the approaching fire front as expected. We hypothesise that this is due to stronger ambient winds that advected hot gases forward and downwind of the fire front, which established lower pressure ahead of the front and resulted in acceleration of air through the flame front, limiting acceleration in the opposite direction.

Although this experiment provides an unprecedented dataset for analysis and model evaluation studies, there are some caveats that need to be mentioned. First, the airborne IR imagery was saturated, which limited its use in determining the fire behaviour characteristics of the entire burn unit. Additionally, the position of both the airborne and tower-based IR camera systems were such that only the first few minutes of the fire's progression provided reliable fire front position estimates. Although this failure is problematic for estimating fine-scale fire behaviour properties, the *in situ* sensors do provide a redundant source of information that can be used for analyses and model comparisons.

Overall, the experiment was successful in that it collected a large set of micrometeorological, air chemistry and fire behaviour data under high fire danger conditions. We show that the use of a coupled fire–atmosphere modelling system can assist in the design of even a small-scale experiment by helping determine fire front positions and where to ideally place *in situ* instrumentation to capture fire behaviour and to carry out near-surface meteorological measurements. These data will provide a valuable dataset for not only the testing coupled fire–atmosphere models, but the large amount of turbulence measurements will be invaluable for future analyses of turbulence regimes that develop in the vicinity of fires. Future experiments should utilise fine-scale modelling to help design field campaigns and to determine best-case scenarios for forecast wind conditions. Future experiments should also be flexible in their instrument installation layout in order to adapt to potential changes in meteorological conditions. The data collected during this experiment are available for use by request at http://www.fireweather.org/data-request/.

Conflicts of interest

The authors declare no conflicts of interest.

Declaration of funding

This research was funded by the National Science Foundation (AGS-1151930), the Joint Fire Science Program (11–2-1–11), and the USFS Northern Research Station (13-CR-11242306–073).

Acknowledgements

Many individuals were involved in making this experiment a success and the authors would like to acknowledge them here. First, we thank the burn boss, Rich Gray from the Texas A&M Forest Service and his burn crew who made all the preparations and conducted all the firing operations. We also want to thank David Popoff from Galveston County Emergency Management Division and Captain Todd Weidman from La Marque Fire Department for helping organise the burn experiment and handling much of the incident coordination. We thank Kent Prochazka from the NWS Galveston Forecast Office for providing the spot weather forecasts. Additionally, Mike Wotton (Canadian Forest Service and University of Toronto) kindly lent 10 HOBO data loggers and thermocouples to the experiment. The authors thank the staff at the HCC, especially Mr Tim Becker for his help in preparing the field site and managing our storage needs. Bill O'Shaughnessy is thanked for designing and building the custom pressure sensor packages. We want to also thank the three anonymous reviewers for their comments, which greatly improved this manuscript. The authors would like to acknowledge the

computing resources made available for this project by the Center of High Performance Computing at the University of Utah, as well the Center for Computational Mathematics, Department of Mathematical and Statistical Sciences, at the University of Colorado Denver.

References

Achtemeier GL (2013) Field validation of a free-agent cellular automata model of fire spread with fire–atmosphere coupling. *International Journal of Wildland Fire* **22**, 148–156. doi:10.1071/WF11055

Achtemeier GL, Goodrick SA, Liu Y, Garcia-Menendez F, Hu Y, Odman MT (2011) Modeling smoke plume-rise and dispersion from southern United States prescribed burns with Daysmoke. *Atmosphere* **2**, 358–388. doi:10.3390/ATMOS2030358

Adams JS, Williams DW, Tregellas-Williams J (1973) Air velocity, temperature, and radiant-heat measurements within and around a large free-burning fire. In '14th International Symposium on Combustion', 20–25 August 1972. Vol. 14(1) pp. 1045–1052. https://doi.org/10.1016/S0082-0784(73)80094-3 (The Combustion Institute: Pittsburgh, PA, USA)

Andrews PL (2014) Current status and future needs of the BehavePlus fire modeling system. *International Journal of Wildland Fire* **23**, 21–23. doi:10.1071/WF12167

Bradski G, Kaehler A (2008) 'Learning OpenCV: computer vision with the OpenCV Library.' (O'Reilly Media, Inc.: Sebastopol, CA, USA)

Butler B, Teskey C, Jimenez D, O'Brien J, Sopko P, Wold C, Vosburgh M, Hornsby B, Loudermilk E (2016) Observations of energy transport and spread rates from low-intensity fires in longleaf pine habitat – RxCADRE 2012. *International Journal of Wildland Fire* **25**, 76–89. doi:10.1071/WF14154

Cheney NP, Gould JS (1995) Fire growth in grassland fuels. *International Journal of Wildland Fire* **5**, 237–247. doi:10.1071/WF9950237

Cheney NP, Gould JS, Catchpole WR (1993) The influence of fuel, weather and fire shape variables on fire spread in grasslands. *International Journal of Wildland Fire* **3**, 31–44. doi:10.1071/WF9930031

Cheney NP, Gould JS, McCaw WL, Anderson WR (2012) Predicting fire behaviour in dry eucalypt forest in southern Australia. *Forest Ecology and Management* **280**, 120–131. doi:10.1016/J.FORECO.2012.06.012

Clements CB, Oliphant A (2014) The California State University Mobile Atmospheric Profiling System: a facility for research and education in boundary-layer meteorology. *Bulletin of the American Meteorological Society* **95**, 1713–1724. doi:10.1175/BAMS-D-13-00179.1

Clements CB, Seto D (2015) Observations of fire–atmosphere interactions and near-surface heat transport on a slope. *Boundary-Layer Meteorology* **154**, 409–426. doi:10.1007/S10546-014-9982-7

Clements CB, Zhong S, Goodrick S, Li J, Bian X, Potter BE, Heilman WE, Charney JJ, Perna R, Jang M, Lee D, Patel M, Street S, Aumann G (2007) Observing the dynamics of wildland grass fires: FireFlux – a field validation experiment. *Bulletin of the American Meteorological Society* **88**, 1369–1382. doi:10.1175/BAMS-88-9-1369

Clements CB, Lareau N, Seto D, Contezac J, Davis B, Teske C, Zajkowski TJ, Hudak A, Bright B, Dickenson MB, Butler B, Jimenez D, Heirs JK (2016) Fire weather conditions and fire–atmosphere interactions observed during low-intensity prescribed fires – RxCADRE 2012. *International Journal of Wildland Fire* **25**, 90–101. doi:10.1071/WF14173

Countryman CM (1969) Project Flambeau. An investigation of mass fire (1964–1967). Final report – Vol. I. USDA Forest Service, Pacific Southwest Forest and Range Experiment Station, pp. 1–68. (Berkeley, CA, USA)

Dupuy J-L, Pimont F, Linn RR, Clements CB (2014) FIRETEC evaluation against the FireFlux experiment: preliminary results. In 'VII International conference on forest fire research proceedings', 17–20 November 2014, Coimbra, Portugal. (Ed. Viegas DX) pp. 261–274. doi: 10.14195/978-989-26-0884-6_28 (Imprensa da Universidade de Coimbra: Coimbra, Portugal)

Filippi J-B, Pialat X, Clements CB (2013) Assessment of ForeFire/Meso-NH for wildland fire/atmosphere coupled simulation of the FireFlux experiment. *Proceedings of the Combustion Institute* **34**, 2633–2640. doi:10.1016/J.PROCI.2012.07.022

Finney MA (1998) FARSITE: Fire Area Simulator – model development and evaluation. USDA Forest Service, Rocky Mountain Research Station, Research Paper RMRS-RP-4, p. 47. (Ogden, UT, USA)

Finney MA, Cohen J, Forthofer J, McAllister S, Gollner MJ, Gorham D, Saito K, Adam B, English J (2015) The influence of buoyant dynamics on wildfire spread. *Proceedings of the National Academy of Sciences of the United States of America* **112**, 9833–9838. doi:10.1073/PNAS.1504498112

FIRESCAN Science Team (1996) Fire in ecosystems of boreal Eurasia: the Boreal Forest Island Fire Experiment, Fire Research Campaign Asia–North (FIRESCAN). In 'Biomass burning and global change. Vol. 2. Biomass burning in South America, south-east Asia, and temperate and boreal ecosystems, and the oil fires of Kuwait'. (Ed. JS Levine) pp. 848–873. (MIT Press: Cambridge, MA, USA)

Gould JS, McCaw WL, Cheney NP, Ellis PF, Knight IK, Sullivan AL (2007) 'Project Vesta – Fire in dry eucalypt forest: fuel structure, fuel dynamics and fire behaviour.' (Ensis–CSIRO: Canberra, ACT, Australia; and Department of Environment and Conservation: Perth, WA, Australia)

Hinzman L, Fukuda M, Sandberg DV, Chapin FS, III, Dash D (2003) FROSTFIRE: an experimental approach to predicting the climate feedbacks from the changing boreal fire regime. *Journal of Geophysical Research* **108**, 8153. doi:10.1029/2001JD000415

Kochanski AK, Jenkins M, Mandel J, Beezley J, Clements CB, Krueger S (2013) Evaluation of WRF-Sfire performance with field observations from the FireFlux experiment. *Geoscientific Model Development* **6**, 1109–1126. doi:10.5194/GMD-6-1109-2013

Linn RR, Anderson K, Winterkamp J, Brooks A, Wotton M, Dupuy J-L, Pimont F, Edminster C (2012) Incorporating field wind data into FIRETEC simulations of the International Crown Fire Modeling Experiment (ICFME): preliminary lessons learned. *Canadian Journal of Forest Research* **42**, 879–898. doi:10.1139/X2012-038

Mandel J, Beezley JD, Kochanski AK (2011) Coupled atmosphere–wildland fire modeling with WRF 3.3 and SFIRE 2011. *Geoscientific Model Development* **4**, 591–610. doi:10.5194/GMD-4-591-2011

McRae DJ (1996) Prescribed fire aerial ignition strategies. Natural Resources Canada, Canadian Forest Service, Great Lakes Forestry Centre, NODA/NFP Technical Report TR-33. (Sault Sainte Marie, ON, Canada)

Mell W, Jenkins M, Gould J, Cheney P (2007) A physics-based approach to modelling grassland fires. *International Journal of Wildland Fire* **16**, 1–22. doi:10.1071/WF06002

Ottmar RD, Hiers JK, Clements CB, Butler B, Dickinson MB, Potter B, O'Brien JJ, Hudak AT, Rowell EM, Zajkowski TJ (2016) Measurements, datasets and preliminary results from the RxCADRE project. *International Journal of Wildland Fire* **25**, 1–9. doi:10.1071/WF14161

Palmer TY (1981) Large fire winds, gases and smoke. *Atmospheric Environment* **15**, 2079–2090. doi:10.1016/0004-6981(81)90241-9

Quintiere JG (1993) Canadian mass fire experiment. *Journal of Fire Protection Engineering* **5**, 67–78. doi:10.1177/104239159300500203

Rothermel RC (1972) A mathematical model for predicting fire spread in wildland fuels. USDA Forest Service, Intermountain Forest and Range Experiment Station, Research Paper INT-RP-115. (Ogden, UT, USA).

Schroeder MJ, Countryman CM (1960) Exploratory fire climate surveys on prescribed burns. *Monthly Weather Review* **88**, 123–129. doi:10.1175/1520-0493(1960)088<0123:EFSOPB>2.0.CO;2

Simard AJ, Eenigenburg JE, Adams KB, Nissen RL, Deacon AG (1984) A general procedure for sampling and analyzing wildland fire spread. *Forest Science* **30**, 51–64.

Stocks BJ, McRae DJ (1991) The Canada/United States cooperative mass fire behaviour and atmospheric environmental impact study. In

'Proceedings of the 11th conference on fire and forest meteorology', 16–19 April 1991, Missoula, MT. (Eds PL Andrews, DF Potts) pp. 478–487. (Society of American Foresters: Bethesda, MD, USA)

Stocks BJ, van Wilgen BW, Trollope WSW, McRae DJ, Mason JA, Weirich F, Potgieter AIF (1996) Fuels and fire behaviour dynamics on large-scale savanna fires in Kruger National Park, South Africa. *Journal of Geophysical Research* **101**, 23541–23550. doi:10.1029/95JD01734

Stocks BJ, Alexander ME, Wotton BM, Stefner CN, Flannigan MD, Taylor SW, Lavoie N, Mason JA, Hartley GR, Maffey ME, Dalrymple GN, Blake TW, Cruz MG, Lanoville RA (2004) Crown fire behaviour in a northern jack pine–black spruce forest. *Canadian Journal of Forest Research* **34**, 1548–1560. doi:10.1139/X04-054

Sullivan AL (2009) Wildland surface fire spread modelling, 1990–2007. 3: Simulation and mathematical analogue models. *International Journal of Wildland Fire* **18**, 387–403. doi:10.1071/WF06144

Taylor RJ, Evans ST, King NK, Stephens ET, Packham DR, Vines RG (1973) Convective activity above a large-scale bushfire. *Journal of Applied Meteorology* **12**, 1144–1150. doi:10.1175/1520-0450(1973)012<1144:CAAALS>2.0.CO;2